The BINGO/ABDUS Project:

Forecast for cosmological parameter from a mock Fast Radio Bursts survey

Xue Zhang ⋆[1], Yu Sang ⋆⋆[1], Gabriel A. Hoerning ⋆⋆⋆[2], Filipe B. Abdalla ⋆⋆⋆⋆[3, 4, 5, 2, 6], Elcio Abdalla[2, 7, 8], Amilcar Queiroz[9], André A. Costa[1, 10, 11, 12], Ricardo G. Landim[13, 14], Chang Feng[3, 4, 5], Bin Wang[1, 15], Marcelo V. dos Santos[9, 2], Thyrso Villela[16, 17, 18], Carlos A. Wuensche[16], Jiajun Zhang[19], Edmar Gurjão[20], Alessandro Marins[3], Alexandre Serres[20], and Linfeng Xiao[21]

(Affiliations can be found after the references)

ABSTRACT

Context. There are hosts of surveys that will provide excellent data to search for and locate Fast Radio Bursts (FRBs) at cosmological distances. The BINGO project is one such surveys, and this collaboration has already estimated a FRB detection rate that the project will yield with the main telescope helped by a set of outrigger stations.

Aims. This paper aims to simulate and estimate the potential of FRBs in constraining our current cosmological model. We present a forecast of the future constraints that the BINGO FRB detections and localizations will have when added to other current cosmological datasets.

Methods. We quantify the dispersion measure (DM) as a function of redshift (z) for the BINGO FRB mock sample. Furthermore, we use current datasets (Supernovae, Baryonic Acoustic Oscillations, and Cosmic Microwave Background data) prior to assessing the efficacy of constraining dark energy models using Monte Carlo methods.

Results. Our results show that spatially located BINGO FRB dataset will provide promising constraints on the population of host galaxies intrinsic DM and be able to measure the nuisance parameters present within a FRB cosmological analysis. Still, they will also provide alternative estimates on other parameters such as the Hubble constant and the dark energy equation of state. In particular, we should see that BINGO FRB data can put constraints on the degenerate $w - H_0$ plane, which the CMB is incapable of measuring, allowing FRBs to be a viable alternative to BAO to constrain the dark energy equation of state.

Conclusions. We conclude that FRBs remain a promising future probe for cosmology and that the FRBs detected by the BINGO project will contribute significantly to our knowledge of the current cosmological model.

Key words. Fast Radio Burst; cosmological constraints

1. Introduction

Fast Radio Bursts (FRBs) were discovered while analyzing previous radio data from Parkes radio telescope and reported in Lorimer et al. (2007). Since the first discovery of FRBs, a number of events have been observed by several radio telescopes over the world (Thornton et al. 2013; Spitler et al. 2016; Chatterjee et al. 2017; Bochenek et al. 2020; Tendulkar et al. 2017). Such an important discovery led to a new field in astronomy and physics, namely the discovery, distribution, location, and properties of these extremely energetic objects. From the point of view of astrophysics, the intrinsic behavior, properties, origin, and theoretical description of FRBs are of utmost importance (Cordes & Chatterjee 2019; Petroff et al. 2019, 2022).

FRBs are radio transients with milliseconds duration. Their distances are estimated from the dispersion measure (DM), which corresponds to the time distribution in frequency space (Lorimer et al. 2007; Dennison 2014; Caleb et al. 2016). This is due to the passage of the wave train in the intergalactic medium, which is constituted of electrons, implying slightly different velocities according to the frequency as a consequence of electromagnetic interaction. The large DMs imply that the sources are

at cosmological distance (Keane et al. 2012; Xu & Han 2015; Chatterjee et al. 2017; Tendulkar et al. 2017). Combined with the redshifts of their host galaxies, the DM of FRBs provides a new tool to investigate the structure of the Universe, including constraining the location of the "missing baryons", probing the properties of the very diffuse intergalactic medium (IGM) and circumgalactic medium (CGM) around galaxies (Bhandari & Flynn 2021; McQuinn 2014; Ravi 2019; Lin & Sang 2021).

The progenitors of FRBs are still a mystery to the astronomical community. Some theoretical models have been proposed to explain the origin of FRBs (Platts et al. 2019; Zhang 2023); some possible progenitor candidates are compact object mergers (Totani 2013; Wang et al. 2016b), the collapse of compact objects (Falcke & Rezzolla 2014; Zhang 2014), supernovae remnants (Keane et al. 2012; Cordes & Wasserman 2016; Connor et al. 2016), and active galactic nuclei (Romero et al. 2016; Vieyro et al. 2017). Utilizing the rapidly accumulating observational data of FRBs (Amiri et al. 2021, 2024; Xu et al. 2023; Petroff et al. 2016), the statistical properties of the key observed quantities, such as energy and waiting time, are extensively analyzed, yielding critical insights for investigating the origins and physical mechanisms of FRBs (Law et al. 2017; Lin & Sang 2020; Sang & Lin 2022; Wang et al. 2023b; Sang & Lin 2023, 2024; Wang & Yu 2017; Hashimoto et al. 2022).

It is also possible to apply FRBs surveys to the field of cosmology to study various critical issues, such as dark energy mod-

⋆ zhangxue@yzu.edu.cn
⋆⋆ sangyu@yzu.edu.cn
⋆⋆⋆ ghoerning@usp.br
⋆⋆⋆⋆ filipe.abdalla@gmail.com

els (Walters et al. 2018; Zhao et al. 2020; Qiu et al. 2022; Zhao et al. 2023; Zhang et al. 2023), ionized gas fraction (Jaroszynski 2019; Walters et al. 2019; Yang & Zhang 2016; Lin & Sang 2021), spatial curvature density (Yu & Wang 2017; Walters et al. 2018), cosmic baryon density (Macquart et al. 2020; Qiang & Wei 2020), the baryon fraction in the IGM (Lemos et al. 2023a,b), Hubble parameter (Wu et al. 2020; Zhang et al. 2023), as well as other cosmological questions (Qiang et al. 2020; Lin et al. 2023; Walker et al. 2020; Zhu & Zhang 2022). The cosmological origin of FRBs is confirmed by identifying the host galaxy and its redshift measurement from other wavebands. The redshift is essential for probing the Universe using FRBs. If it is possible to locate the host of the FRB, one can foresee using the relation between the DM estimated from this object and the redshift of the host galaxy. This would permit further constraints in the cosmological parameters, which today is one of the paths towards understanding and improving our cosmological description, including the description of the Dark Sector of the Universe (Abdalla & Marins 2020).

The aim of the BINGO (BAO from Integrated Neutral Gas Observations) telescope was primarily to inquire about the aforementioned constraints on cosmological parameters (Abdalla et al. 2022a; Costa et al. 2022; Abdalla et al. 2022b; Wuensche et al. 2022). With the further development of the ABDUS (Advanced Bingo Dark Universe Studies) as an extension to BINGO (Abdalla et al. 2024), it is clear that constraints on the FRBs parameters can become much more important and accurate, enabling a deeper view of the Universe details and a stronger constraint on the cosmological parameters as described above.

There are 23 FRBs whose host galaxies have measured redshifts (see Wang et al. (2023a) and references therein). When detected by a single radio telescope, the FRB signal will probably be located within the primary beam of the instrument, posing an observational difficulty due to their usually large beams. As a consequence, the host galaxy cannot always be accurately identified. However, localizations can likely be accurately produced in the radio band by performing an interferometric detection of a given FRB candidate in more than two instruments. Once the FRB is accurately localized, it is easy to match the FRB source with galaxy surveys and identify its host galaxy.

The aim of this paper is to demonstrate the ability to constrain cosmology using FRBs detected by ABDUS (Abdalla et al. 2024). To achieve this goal, in a previous BINGO project IX paper, a BINGO/ABDUS Interferometry System (BIS) [1] has been proposed to find the FRB sources in the sky via fringe fitting between the main telescope and the outriggers (dos Santos et al. 2024); hundreds of FRB detections and localizations are feasible. The simulation data produced in this previous work is used here as our mock for FRBs. With this framework, we will be able to show the cosmological advances that are possible with this dataset.

This paper is organized as follows: in Section 2, we outline the methodology used in this paper; in Section 3, we present the results of our simulations and how they improve current cosmological parameter constraints in current dataset; then we discuss the conclusions of our findings in Section 4.

---

[1] In this work, we adopt the term 'BINGO' to refer to the BINGO/ABDUS Interferometry System for convenience.

2. Methodology and data

2.1. The Dispersion Measure

FRBs are transient radio sources that commonly have extragalactic origin. The searches for FRBs are generally done by assembling many time series. When a FRB is detected, we observe a sharp pulse with dispersion effects at different frequencies. During the traveling from the FRB source to the telescope through an ionized medium, the radio photons interact with ionized matter, causing a time delay in the propagation of the pulse signal. The radio pulse is thus dispersed when traveling in the ionized intergalactic medium. The dispersion is quantified by the time delay of the pulse between the highest and lowest radio frequencies (Petroff et al. 2019),

$$\Delta t = \frac{e^2}{2\pi m_e c}\left(\nu_{\text{low}}^{-2} - \nu_{\text{high}}^{-2}\right)\text{DM} \quad, \tag{1}$$

where Δt is the arrival time delay in the observer frame, ν_{high} and ν_{low} are the highest and lowest radio frequencies of observation, respectively. Also, m_e is the mass of the electron, c is the speed of light, and DM is the dispersion measure. Thus, as the signal travels from the source and traverses the intervening medium to Earth, it directly traces ionized baryons that cannot be detected using other observational methods.

The DM is defined as the integral of the electron number density along the line of sight from the source to the observer,

$$\text{DM} = \int_0^d n_e(l)dl, \tag{2}$$

where n_e is the free electron number density, l is the path length and d is the distance to the source. The DM is usually given in units of pc/cm^3.

The main contributions to observed DM come from the Milky Way (MW) galaxy, intergalactic medium (IGM), and host galaxy (HG). The total DM is the sum of these components:

$$\text{DM} = \text{DM}_{\text{MW}} + \text{DM}_{\text{IGM}} + \frac{\text{DM}_{\text{HG}}}{1+z}, \tag{3}$$

where DM_{MW} represents the amount of dispersion from the Milky Way. It includes contributions of free electrons from the interstellar medium (ISM) and the Galactic halo. The ISM part is derived from an electron distribution model, NE2001 (Cordes & Lazio 2002, 2003) or YMW16 (Yao et al. 2017), and the halo component has been estimated by numerous studies (Prochaska & Zheng 2019; Keating & Pen 2020; Macquart et al. 2020; James et al. 2021; Cook et al. 2023). DM_{IGM} is the contribution from the intergalactic medium, and DM_{HG} is the contribution from the host of the source itself. Due to the expansion of the Universe, the observed DM for the host galaxy is giving by scaled the DM in the host galaxy's rest frame by a factor of $1/(1 + z)$. The DM_{HG} strongly depends on the host galaxy type and its local environment (Tendulkar et al. 2017; Bassa et al. 2017). Following Deng & Zhang (2014), we defined the excess extragalactic contributions DM_{E} as

$$\text{DM}_{\text{E}} \equiv \text{DM} - \text{DM}_{\text{MW}} = \text{DM}_{\text{IGM}} + \frac{\text{DM}_{\text{HG}}}{1+z}. \tag{4}$$

The largest contribution to DM comes from the intergalactic medium, defined as

$$\text{DM}_{\text{IGM}} = \int_0^{z_s} \frac{cH_0 n_e}{(1+z)^2 E(z)}dz, \tag{5}$$

where H_0 is the Hubble constant, $E(z)$ is the dimensionless expansion rate of the Universe at redshift z, and z_s is the redshift of the source.

In the late Universe, the distribution of free electrons is highly inhomogeneous. The electron number density and DM_{IGM} depend on the direction of the sky. To find a relationship between DM and z, we assume the same approach as in Deng & Zhang (2014), where it was assumed that all baryons are homogeneously distributed and ionized with an ionization fraction χ_e. So in practice, we use the average of these values over the sky. The mean number density of free electrons at redshift z is

$$\bar{n}_e(z) = \frac{3H_0^2\Omega_b f_{IGM}}{8\pi G m_p}\chi_e(z)(1+z)^3, \qquad (6)$$

where f_{IGM} is the fraction of baryon mass in the intergalactic medium and is often taken as 0.83. The ionization fraction of free electrons χ_e is

$$\chi_e(z) = Y_H\chi_{e,H}(z) + \frac{1}{2}Y_{He}\chi_{e,He}(z), \qquad (7)$$

where Y_H and Y_{He} are the hydrogen and helium mass fractions. Their mass ratio is approximately $3 : 1$, normalized to 3/4 and 1/4, respectively. For $z \lesssim 3$, the hydrogen and helium are fully ionized. So the ionization fractions are $\chi_{e,H} = \chi_{e,He} = 1$. Hence, the average of the DM from the intergalactic medium can be written as

$$\langle DM_{IGM}(z_s)\rangle = \frac{3cH_0\Omega_b f_{IGM}}{8\pi G m_p}\int_0^{z_s}\frac{\chi_e(z)(1+z)}{E(z)}dz. \qquad (8)$$

Hence, Eq. (8) is a function of cosmological parameters. And if the redshift z is measured, the DM can be used to constrain cosmological parameters.

We assume DM_{IGM} follows a Gaussian distribution

$$DM_{IGM} = N(\langle DM_{IGM}(z_s)\rangle, \sigma_{IGM}), \qquad (9)$$

where the average value of DM_{IGM} is expressed by Eq. (8). The variance of DM_{IGM} is typically assumed to be a constant in the previous literatures. However, here we adopt a more appropriate and complex form where the variance of DM_{IGM} depends on the power spectrum (McQuinn 2014; Walker et al. 2020):

$$\sigma_{IGM}^2(DM, z_s) = \int_0^{\chi_s} d\chi(1+z)^2 \bar{n}_e^2(0) \int \frac{d^2k_\perp}{(2\pi)^2}P_e(k_\perp, z)$$
$$= \frac{c}{H_0}\left[\frac{\chi_e\Omega_b\rho_{cr}}{\mu_e m_p}\right]^2 \int_0^{z_s} dz\frac{(1+z)^2}{E(z)}\int dk k P_e(k, z), \qquad (10)$$

where z_s is the redshift of the source, χ is the comoving distance, χ_s is the comoving distance of the source, ρ_{cr} is the critical density and $\mu_e \simeq 1.14$ is the mean mass per electron. Besides, P_e is the electron power-spectrum assumed to be $P_e(k,z) = b\,P_m(k,z)$, where P_m is the matter power-spectrum and $b \simeq 1$ is a bias factor assumed to be constant.

Currently, there is still limited knowledge about the host term DM_{HG} due to the lack of detailed observation on the local environment of most FRB sources. It is difficult to accurately characterize DM_{HG} because of its large uncertainty and the lack of well-localized FRBs. It may vary in a large range, ranging from several tens to hundreds pc/cm^3 (Xu et al. 2022; Niu et al. 2022). To account for the large variation of DM_{HG}, its distribution is usually modeled by the log-normal function (Macquart et al.

2020; Zhang et al. 2020; Lin & Zou 2024). We adopt the probability distribution of DM_{HG} as follows:

$$P(DM_{HG}) = \frac{1}{\sqrt{2\pi}DM_{HG}\sigma_{host}}\exp\left[-\frac{(\ln DM_{HG} - \mu)^2}{2\sigma_{host}^2}\right], \qquad (11)$$

which is characterized by a median $\exp(\mu)$ and logarithmic width parameter σ_{host}. Currently, there is no strong evidence for the redshift-dependence of μ or σ_{host} (Tang et al. 2023). Thus, we treat these two parameters as free constant parameters, although this could be modified when real data is being analyzed, as we are following a Bayesian approach.

2.2. Cosmological models considered

The dark energy equation of state (EoS) parameter is defined as $w(z) = p_{de}(z)/\rho_{de}(z)$, with pressure $p_{de}(z)$ and density $\rho_{de}(z)$ of dark energy, respectively. In a spatially flat Universe, the dimensionless Hubble expansion rate of the Universe at z is given by the Friedmann equation:

$$E(z) = \frac{H(z)}{H_0} = \sqrt{\Omega_m(1+z)^3 + \Omega_{de}\exp\left[3\int_0^z\frac{1+w(z')}{1+z}dz'\right]}. \qquad (12)$$

Here H_0 is the expansion rate measured today, and $\Omega_{de} = 1 - \Omega_m$ is the dimensionless dark energy density of the Universe, where we consider only flat models in this paper. We assume three cosmological models outlined below:

– the ΛCDM model, $w(z) = -1$, in which the cosmological constant Λ serves as dark energy;

– the wCDM model, $w(z) = w$, characterized by a constant EoS;

– the w_0w_aCDM model, using the CPL parameterization (Chevallier & Polarski 2001; Linder 2003), $w(z) = w_0 + w_a z/(1+z)$, in which dark energy has an evolving EoS characterized by two parameters w_0 and w_a.

We choose the cosmological model of our mock catalog of FRB detection by the BINGO/ABDUS interferometric system to have the same cosmological parameters as the best-fit Planck cosmological fit. Therefore, we take $\Omega_b = 0.0494$, $\Omega_m = 0.3166$ and $H_0 = 67.27$ km/s/Mpc as the fiducial values from Planck team (Aghanim et al. 2020b).

2.3. Detailed FRB mock distribution

In this work, we consider a spatial distribution f_z for the population of cosmological FRBs. Such distribution is assumed to be uniform in co-moving volume (Luo et al. 2018, 2020; Chawla et al. 2022; dos Santos et al. 2024),

$$f_z(z) \equiv \frac{\partial V}{\partial\Omega\partial z} = \frac{c}{1+z}\frac{r^2(z)}{H(z)}. \qquad (13)$$

However, this distribution alone cannot describe the population of observed FRBs at a given redshift. To do so, we need to take into account the particular characteristics of a specific survey.

The interaction between the cosmological information and the telescope design is performed by the Python code FRBlip (dos Santos et al. 2024) from the BINGO collaboration. In summary, the code generates the cosmological population, as Eq.

(13), in a given redshift range, associating each FRB to a luminosity distribution. Then FRBlip makes the interaction of the cosmological population with each of the telescope beams in auto and cross-correlations to calculate the signal-to-noise ratio (S/N) of each FRB in each baseline of the BIS, which is the telescope of interest here. More details, such as system temperature, gain parameters for the simulation, and S/N values to classify the FRBs, can be found in dos Santos et al. (2024).

For this work, we generated a cosmological population in the redshift range of $0 < z < 10$ for 5 years of observation. We also consider three different designs for ABDUS, varying the number of horns and outriggers. We plot in Figs. 1 and 2 the number and the observed simulated distribution for FRBs that can be detected by ABDUS. Notably, as the number of stations and mirror size increases, the telescope can localize more FRBs, and their redshift will be higher. Below, we present the three scenarios we are considering in our analysis:

– Case 1: BINGO Main station + outriggers with 6 m diameter collecting area capable of surveying 10 beams in the sky at different locations ($N_{FRB} = 110$).

– Case 2: BINGO Main station + outriggers with 4 m diameter collecting area capable of surveying 112 beams in the sky at different locations ($N_{FRB} = 451$).

– Case 3: BINGO Main station + outriggers with 6 m diameter collecting area capable of surveying 200 beams in the sky at different locations ($N_{FRB} = 878$).
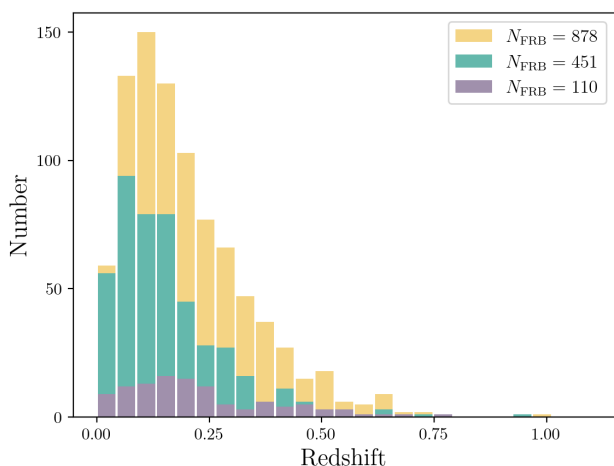
Fig. 1. The mock redshift distribution of the FRB detected by BINGO. The different colors represent different cases for a mock observation with different number of outriggers and outrigger configurations as described in the text, observed over 5 years.

For more details regarding Case 1 we refer the reader to a more detailed explanation of the simulation described in (dos Santos et al. 2024). For both Cases 2 and 3 the set up is similar to Case 1, however both these cases have a larger number of single dish antennas of 4m (Case 2) or 6m (Case 3) diameter. Cases 2 and Cases 3 can also be achieved by data collected by 3 phased array stations with multi-beam capabilities and with same diameters (4m and 6m). When considering the BINGO main telescope simulated data, all the possible auto and cross-correlations with its beams are considered in all cases. Only FRBs localized (with a detected signal to noise) in two or more baselines are used in this analysis, corresponding to the FRBs for which a reliable detection can be achieved.

2.4. Likelihood

The probability density function (PDF) for DM_E can be expressed as follows

$$f(DM_E) = \int_0^{DM_E(1+z)} \frac{1}{\sqrt{2\pi}\sigma_{IGM}} \exp\left[-\frac{(DM_E - \frac{DM_{HG}}{1+z} - \langle DM_{IGM} \rangle)^2}{2\sigma_{IGM}^2}\right]$$
$$\times \frac{1}{\sqrt{2\pi}\sigma_{host} DM_{HG}} \exp\left[-\frac{(\ln DM_{HG} - \mu)^2}{2\sigma_{host}^2}\right] d(DM_{HG}). \tag{14}$$

By setting $x = \ln DM_{HG}$, the above equation changes to

$$f(DM_E) = \int \frac{1}{\sqrt{2\pi}\sigma_{IGM}} \exp\left[-\frac{(DM_E - e^x/(1+z) - \langle DM_{IGM} \rangle)^2}{2\sigma_{IGM}^2}\right]$$
$$\times \frac{1}{\sqrt{2\pi}\sigma_{host}} \exp\left[-\frac{(x-\mu)^2}{2\sigma_{host}^2}\right] dx. \tag{15}$$

We also tested the simplest Gaussian distribution case for DM_{HG}, and the results are shown in the following Subsection 3.4. Using the same method in Macquart et al. (2020), we adopt the likelihood ratio test statistic:

$$\mathcal{D}(\Omega_m, \Omega_b, H_0, 10^9 A_s, n_s, \mu, \sigma_{host}) = 2\log\mathcal{L}_{max}$$
$$-2\log\mathcal{L}(\Omega_m, \Omega_b, H_0, 10^9 A_s, n_s, \mu, \sigma_{host}) \tag{16}$$

where $\mathcal{L}_{max}$ is the maximum likelihood.

To constrain the parameter spaces of the cosmological scenarios, we have used the publicly available Markov Chain Monte Carlo code CosmoMC (Lewis & Bridle 2002; Lewis et al. 2000)[2], which supports the Planck 2018 likelihood (Aghanim et al. 2020a) and additionally has a convergence diagnostic following the Gelman-Rubin statistics (Gelman & Rubin 1992). GetDist [3] is also employed to plot the posterior distributions of the cosmological parameters. We adopt the priors from Table 1 for the parameters mentioned above.

Table 1. List of the fiducial values and prior ranges on the independent parameters using "astro" parameterization in CosmoMC. In addition, we set $\Omega_b H_0$ as a derived parameter.

Parameter	Fiducial value	Prior range
Ω_m	0.3166	[0.01, 0.99]
Ω_b	0.0494	[0.01, 0.1]
H_0	67.27	[20, 100]
$10^9 A_s$	2.101	[1.5, 2.5]
n_s	0.9649	[0.8, 1.2]
e^μ	100	[20, 200]
σ_{host}	1	[0.2, 2]
w (i.e. w_0)	-1	[-3, 0]
w_a	0	[-3, 3]

In our analysis, we note that it is possible to have a negative estimated value of the DM after host galaxy correction (and in a more realistic case after the Milky Way DM correction). This is simply due to statistical errors in the difference between the two quantities. This is largely ignored in this work, and we remove the values that, due to the errors, come across as negative values in our mock catalogs. This should have a minimal impact on the final results as the numbers of FRBs removed are small. In a

---
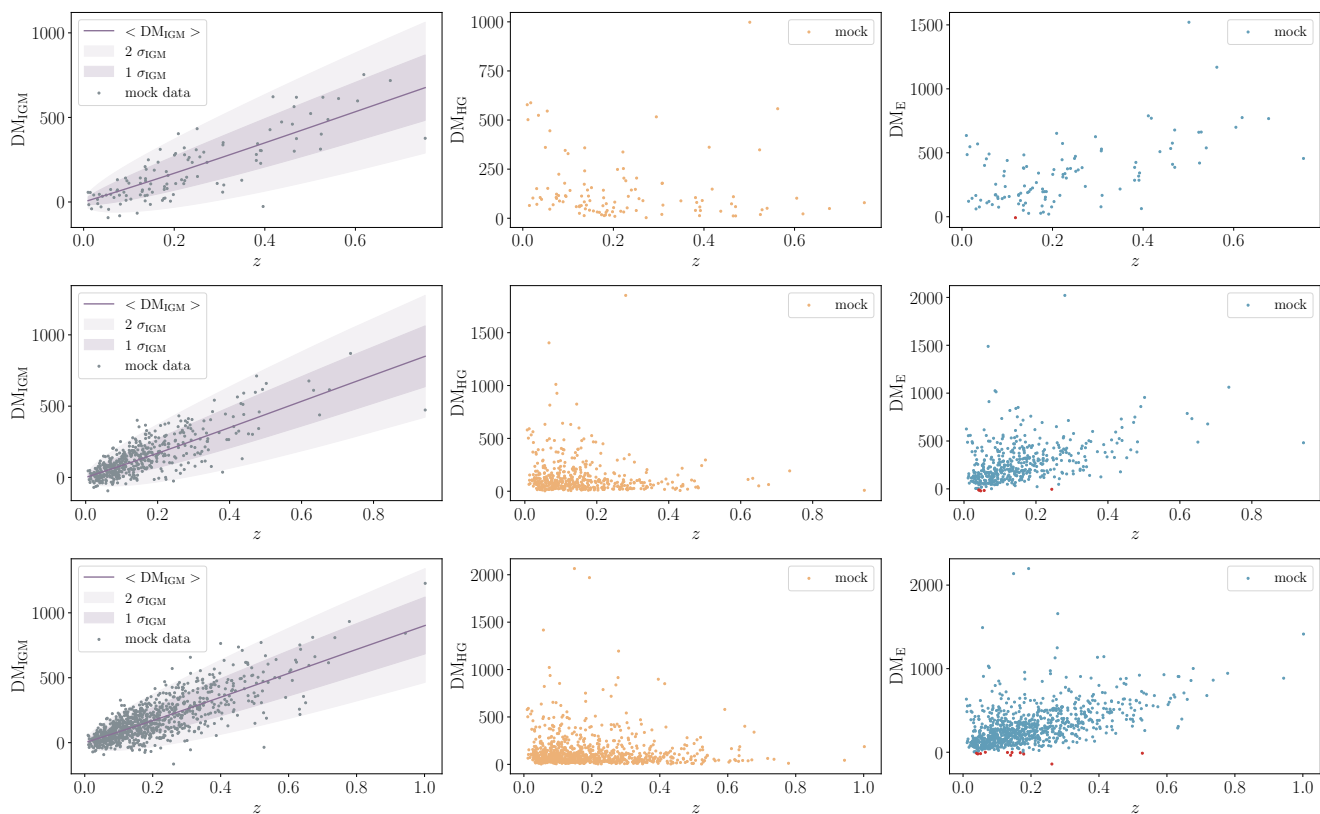
Fig. 2. The simulated FRB data for a 5-year observation of BINGO. The mock data for different cases corresponds to N_{FRB} = 110, 451, 878. The shadows represent the error intervals for the 1σ and 2σ confidence levels. The red dots in the third column indicate that DM_{E} is negative, which is non-physical. Therefore, we removed these points from our later analysis.

realistic scenario, we could use a more sophisticated likelihood to handle such cases, estimating the probability with which such negative values can arise. This approach would involve accounting for the error bars when comparing the extragalactic DM as well as the Milky Way's DM.

2.5. Other observational data

In this section, we describe the other observational datasets that have been used to constrain the underlying cosmological models and the methodology of the statistical simulations. We produce a mix of simulated data combined with real data currently available for cosmological parameter estimation. It is perfectly possible to mix simulated data with real data in order to produce forecasts for future surveys. The observational datasets are there merely to provide constraints that are equivalent to the prior constraints that we would use in a real survey of FRBs. We argue here that this would be the most efficient way of producing such results simply because we know exactly what constraints we obtain from current data from other analyses of each of the collaborations.

It is worth stressing that there is a concern associated with combining real data with simulations. Incompatibility between the datasets can lead to potential discrepancies. For example, it would be very difficult to simulate a mock of what FRBs would yield in terms of detection in the case of CMB data combined with H_0 local measurement data as both datasets are in tension with one another. We, therefore, avoid any such possibilities and remain within the cases where CMB data is compatible with the other datasets used. In other words, it is beyond of the scope of this analysis to identify sources of tension between cosmological

datasets, however it is important to state that a FRB dataset such as the mock we are analysing can potentially help in solving these tensions. Below, we describe the datasets used in the next section of our analysis.

We use the following observational datasets in the analysis:

– Cosmic Microwave Background (CMB): in this work, we utilize the CMB data from the final release by the Planck collaboration. Specifically, we have employed the CMB temperature and polarization power spectra, which include TT-TEEE+lowl+lowE provided by Planck 2018 (Aghanim et al. 2020b).
– Baryon Acoustic Oscillations (BAO): we performed a joint analysis of BAO using various datasets in this work. We specifically combined measurements from the 6dFGS (Beutler et al. 2011), SDSS MGS (Ross et al. 2015), and BOSS DR12 (Alam et al. 2017) as referenced by the Planck 2018 team.
– Supernovae Type Ia (SN Ia): in this study, we utilize a recent dataset of SNIa known as the Pantheon sample (Scolnic et al. 2018), which is distributed across a redshift range of $z \in [0.01, 2.3]$.

3. Results

In this section, we simulate the FRB observations from BINGO in order to constrain the cosmological parameters. The prior ranges of free parameters are listed in Table 1. In addition, we shall compare and combine these obbservations with data from CMB, BAO, and SN Ia datasets. It is worth noting that these constraints are based on observational data, which are used as prior
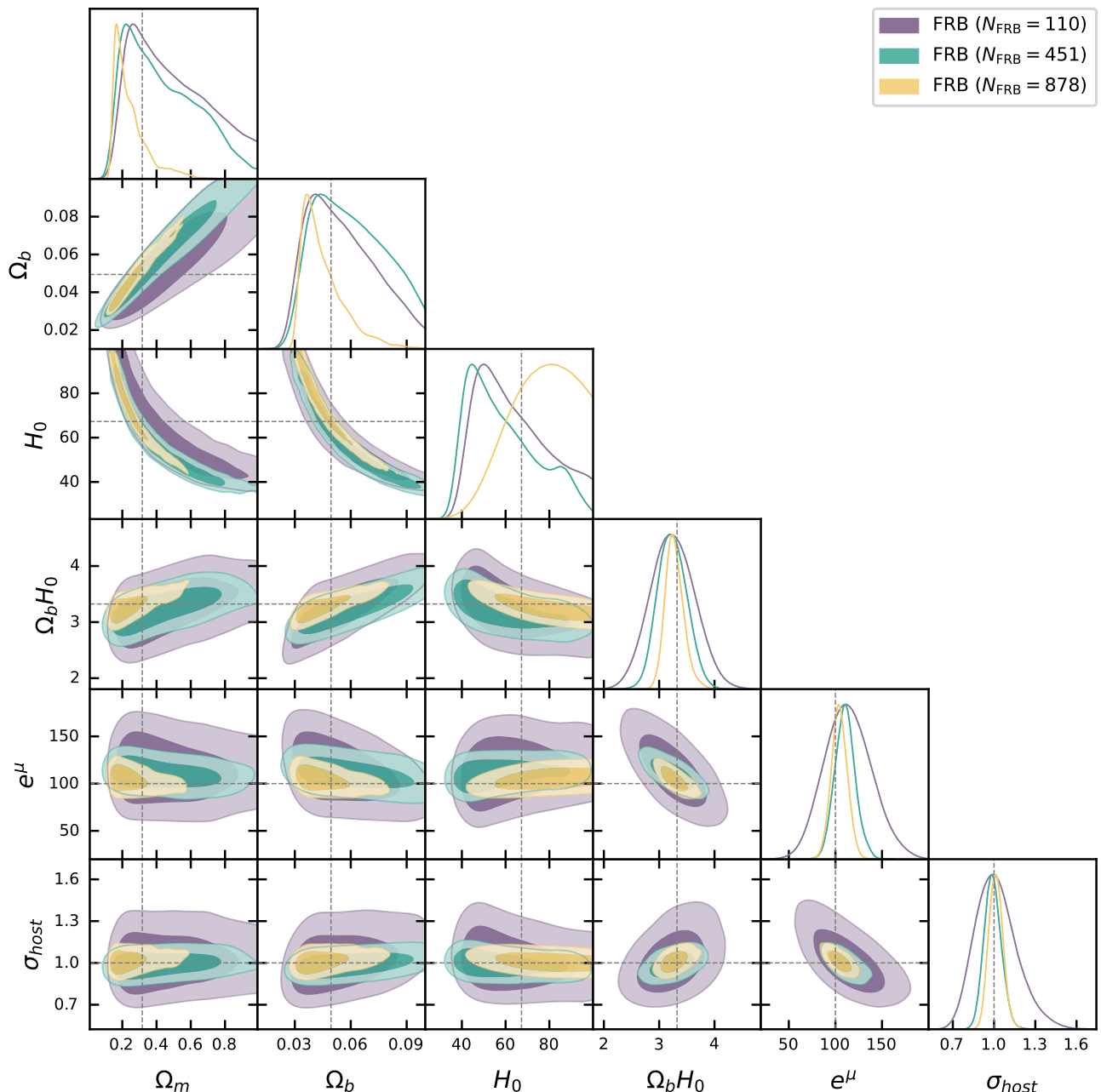
Fig. 3. Constraints of cosmological parameters in ΛCDM model from various case scenarios described in the text for BINGO, varying the number of horns corresponding to $N_{\mathrm{FRB}} = 110$, $N_{\mathrm{FRB}} = 451$ and $N_{\mathrm{FRB}} = 878$. The dashed line stands for the fiducial values we use in this work.

information for our analysis. This approach is valid when there are no significant tensions in the parameters. We will also discuss the constraints on dark energy parameters in ΛCDM, wCDM, and $w_0 w_a$CDM models using our FRB observations.

3.1. Constrains from BINGO FRB alone

In this subsection, we discuss the potential of simulated BINGO FRB data to constrain the aforementioned parameters. First, we emphasize that FRB data will have significant degeneracy alone. If we look at Eq. (8) that describes the dispersion measure of FRBs for the IGM as a function of redshift, we can clearly see that there is a perfect degeneracy between the baryon fraction, the Hubble constant, and the fraction of gas contained within the

IGM. In our analysis, we have chosen f_{IGM} to be constant, as it is perfectly degenerate with H_0 and Ω_b. This is one reason why we choose to express our constraints as the product of $H_0 \times \Omega_b$ in some of our graphs. This shows the power of constraint for FRBs and shows that if FRB cosmology will be able to put constraints on the Hubble constant, it will do so within a factor that depends on our knowledge of f_{IGM}.

Having pointed out the degeneracy issue, we present the FRB-only constraints within the ΛCDM model in Fig. 3. We note that the chosen parameters μ and σ_{host} are nuisance parameters with respect to the modeling of the FRB population distribution. We clearly see that both parameters are reasonably constrained for all simulated BINGO setups. This suggests that, in terms of the statistical power of internally calibrating the mean
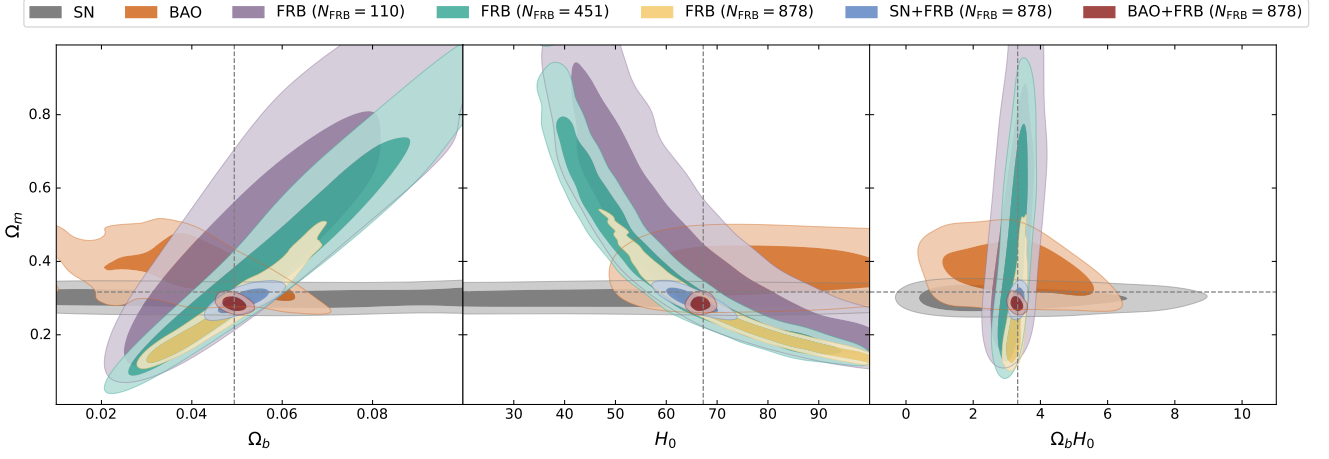
Fig. 4. Constraints (1σ and 2σ confidence level) on Ω_{m}, Ω_{b}, H_0 and $\Omega_{\mathrm{b}}H_0$ for ΛCDM model using the SN, BAO, FRB and their combined dataset. The dashed lines in the three panels indicate the fiducial value chosen for the FRB simulated data, which is consistent with and the same as the Planck best-fit values for ΛCDM parameters.
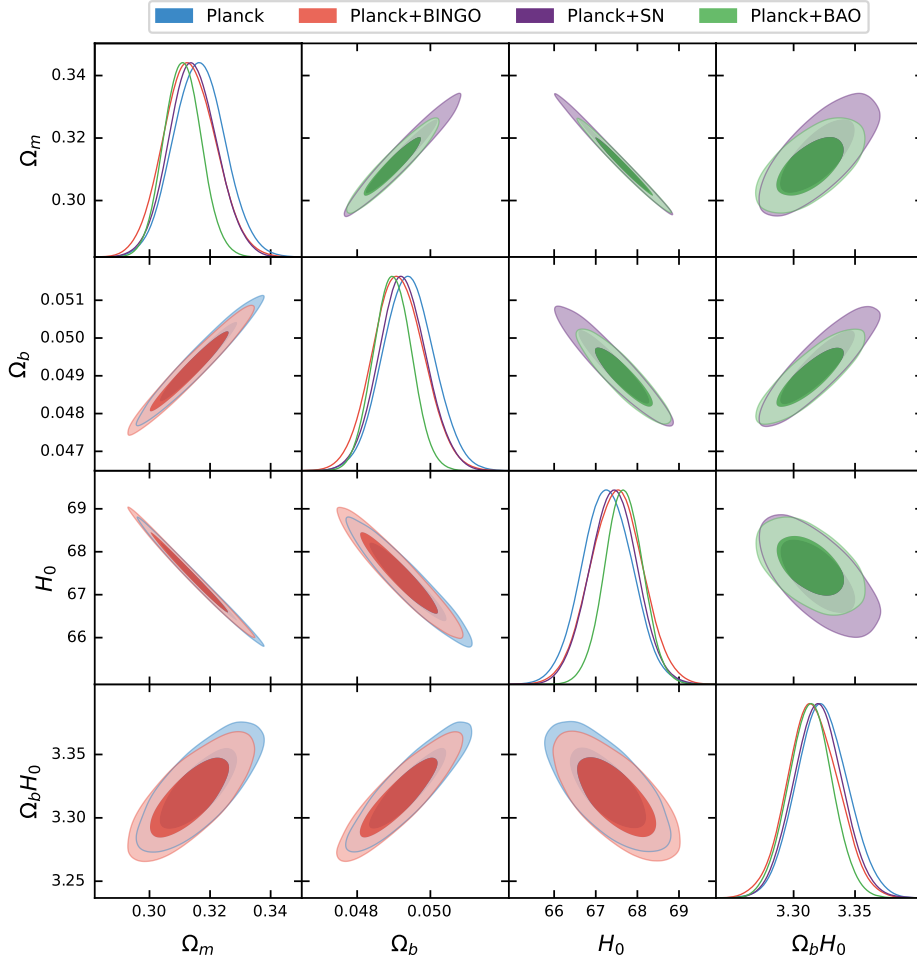
Fig. 5. Constraints (1σ and 2σ confidence level) on Ω_{m}, Ω_{b}, H_0 and $\Omega_{\mathrm{b}}H_0$ for ΛCDM model using the CMB, CMB+FRB, CMB+SN and CMB+BAO data. Here 'BINGO' denote the FRB ($N_{\mathrm{FRB}} = 878$) case.

value for the $\mathrm{DM}_{\mathrm{HG}}$ within the host galaxies, as well as its associated scatter, our model presents reliable results.

We can see that there is a good constraint on the product of $\Omega_{\mathrm{b}} \times H_0$ and that for enough FRB detections, there is a reasonable constraint on Ω_{m} for a ΛCDM cosmology. This suggests

that, when combined with cosmological probes mentioned in Sec. 2.5, FRB data has the potential of helping to put constraints in different cosmological models.

Table 2. 68% constraints on the free and derived parameters of the ΛCDM model using several observational datasets.

Parameters	Planck	Planck+BINGO	Planck+SN	Planck+BAO	SN+BINGO	BAO+BINGO
$\Omega_{\rm m}$	$0.3165^{+0.0083}_{-0.0084}$	$0.3132^{+0.0082}_{-0.0081}$	$0.3144^{+0.0076}_{-0.0081}$	$0.3110^{+0.0061}_{-0.0062}$	$0.2960^{+0.0214}_{-0.0219}$	$0.2870^{+0.0118}_{-0.0168}$
$\Omega_{\rm b}$	0.04940 ± 0.00069	$0.04913^{+0.00067}_{-0.00068}$	0.04925 ± 0.00065	$0.04897^{+0.00051}_{-0.00052}$	$0.05130^{+0.00326}_{-0.00362}$	$0.04933^{+0.00168}_{-0.00170}$
H_0	$67.28^{+0.61}_{-0.60}$	$67.51^{+0.62}_{-0.60}$	$67.43^{+0.56}_{-0.57}$	$67.67^{+0.46}_{-0.45}$	$65.07^{+2.95}_{-3.17}$	$66.78^{+1.16}_{-1.26}$
$\Omega_{\rm b}H_0$	3.323 ± 0.021	3.316 ± 0.020	3.320 ± 0.020	3.314 ± 0.018	$3.329^{+0.127}_{-0.126}$	$3.294^{+0.115}_{-0.117}$

3.2. Comparison with BAO, SNIa, and CMB

We now turn our attention to studying how the FRB data can enhance or constrain the current cosmological ΛCDM model given the cosmological datasets mentioned in Sec. 2.5. We plot our results in Figs. 4 and 5, and Table 2 depicts the best fit of cosmological parameters in our investigation.

In Fig. 4, we can see that there are degeneracy constraints that are significantly orthogonal in the BINGO, BAO, and SNIa datasets when looking at the $\Omega_{\rm m}$ versus $\Omega_{\rm b}H_0$ plane. This means that the combination of these data can potentially yield interesting information to confirm the data constraints from Planck even within a ΛCDM scenario. In the central panel ($H_0 \times \Omega_{\rm m}$) that a combination of the distance measures arising from FRB, SNIa, and BAO can yield an interesting and novel constraint on the Hubble constant. This might be of interest, especially given the Hubble tension that exists in the current cosmological data. It is important to note that these constraints rely on choosing the fiducial value of $f_{\rm IGM}$, with an upper limit $f_{\rm IGM} = 1$. This means that, even considering this astrophysical nuisance parameter, we should be able to add information to investigate the Hubble tension with a future combination of distance measures, including FRB data.

Notably, the red and blue contours suggest that the BINGO FRB constraints are highly complementary to the SNIa and BAO constraints. We note that the BAO + BINGO constraint is somewhat lower than the nominal simulated value for the matter density. This is possible because we have used the Planck central values as the fiducial values for the BAO constraints, rather than the combined Planck + BAO central value. The discrepancy is small enough, and within the error bars in Table 2, and we are not concerned about it in this work.

In Fig. 5, we notice that, for the ΛCDM model, the quality of the Planck data is such high that the other cosmological probes used in this work add very little to the cosmological information brought by Planck only. FBR data marginally improve the cosmological contours, and it is remarkable in the case of Planck combined with BINGO FRB simulated datasets. BAO and SNIa Pantheon data also minimally contribute to improvement of cosmological constraints, as can be seen from the data in Table 2.

3.3. wCDM and w_0w_aCDM model

In the following, we discuss the constraints on the EoS of dark energy by using the FRB data. In Figs. 6 and 7, we show our constraint results on dark-energy EoS parameters for the wCDM and w_0w_aCDM models, respectively.

For the wCDM model, Planck CMB measurements cannot constrain the EoS parameter of dark energy. By combining the CMB data with the simulated FRB samples, we note that, whereas the ΛCDM model for Planck is constrained in a very accurate way, this is not true for the case of wCDM model, where there is a long degeneracy for various values of w. Furthermore, it is shown that this long degeneracy can be broken by the measurements of one of the other cosmological parameters, which
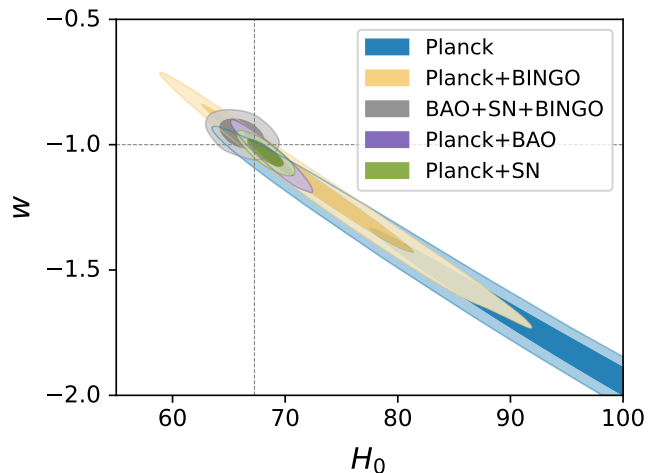

Fig. 6. Comparison between Planck, Planck+BINGO, BAO+SN+BINGO, Planck+BAO and Planck+SN coinstraints in a wCDM model. The dashed line indicates $w = -1$, which corresponds to the standard ΛCDM model. We note that the BINGO FRB mock constraints are able to constrain a combination of the w and H_0 parameters without using any CMB data, which indicates this will be a powerful dataset to help clarify any hubble tension in future datasets.

is why BAO or SNIa do manage, in conjunction with the CMB, to put constraints on the equation of state. Our results show that the BINGO FRB constraints can perform in a similar light to the BAO or SNIa constraints. In our results, shown in Fig. 6, we can see that the degeneracy from the Planck results is cut by the inclusion of the BINGO FRB dataset. Therefore, we can conclude that the results show good prospects for this, but it is possible that another tension might shed some light on the Hubble tension.

The results are similar but somewhat more complex for the case of w_0w_aCDM model. As we know, the recent DESI results show a preference for a Universe where the equation of state parameter varies with redshift. For the w_0w_aCDM model, the CMB data alone can not provide a result of (w_0, w_a) and the best fit for Planck data even falls away from the ΛCDM scenario. These results need to be confirmed but it is possible that another tension might be appearing in our cosmological model. We present the results demonstrating how BINGO could complement CMB data and compare it with the findings of DESI added to the same Planck data. We can see from the left plot in Fig. 7 that the BINGO FRB results will be able to start casting light on the confirmation of the constraints for the CPL parameterization of the dark energy.

The present research also aims at studying the deep structure of the Dark Sector, especially a possibility of interacting dark energy and dark matter, implying a possible nontrivial extension of the elementary particles constitution to contain the Dark Sector (Wang et al. 2016a, 2024). The possibility of a nontrivial dark energy equation of state is a step in that direction.
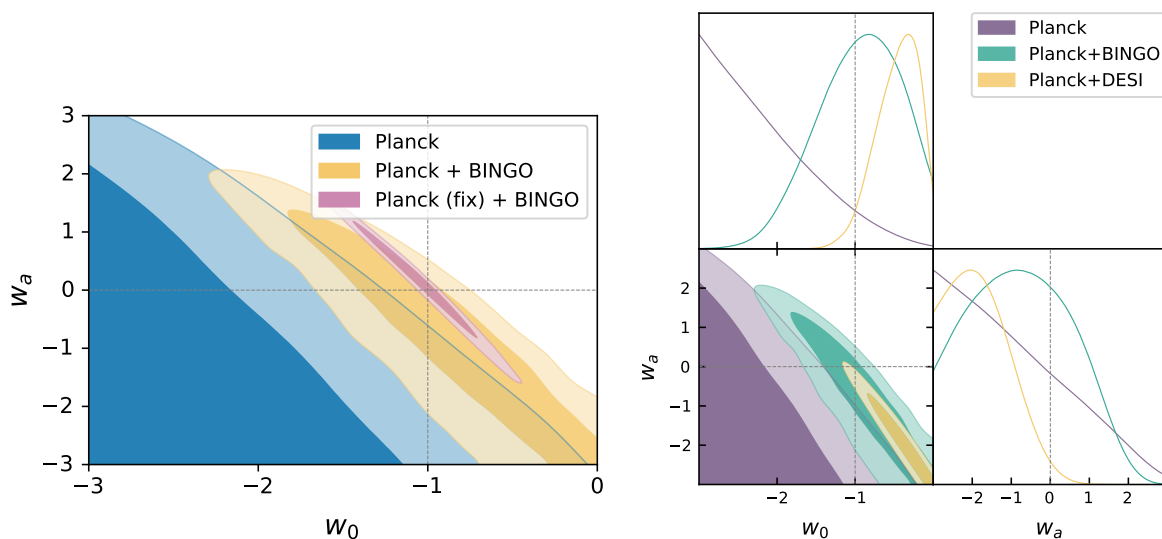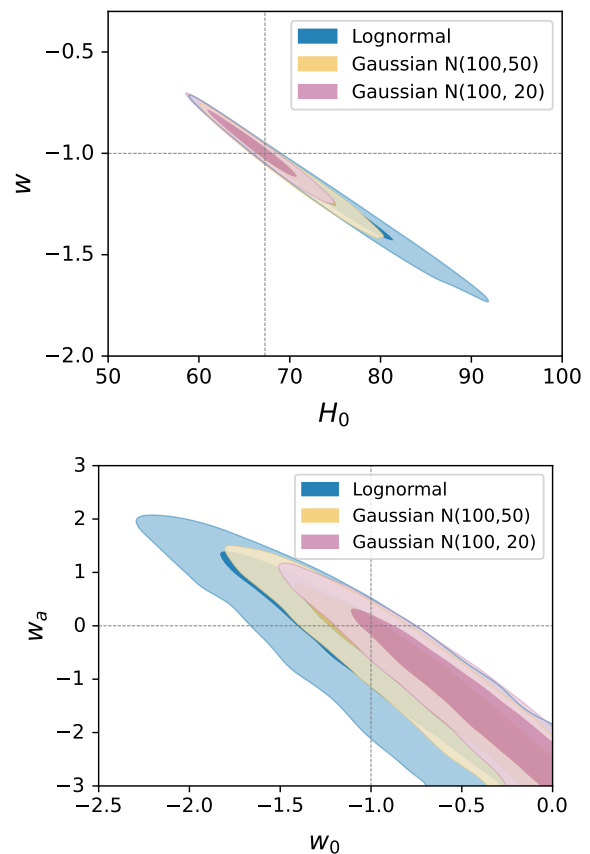
Fig. 7. Marginalized posterior distributions of the (w_0, w_a) parameters are compared for various data combinations in the CPL model, including Planck-only, Planck+BINGO, and Planck (fix)+BINGO. Planck (fix) refers to fixing the cosmological parameters derived by Planck and only setting w_0 and w_a free. Also, the posterior distribution and correlation contour plot of parameters w_0 and w_a in the w_0w_aCDM model are generated using datasets from Planck, Planck+BINGO, and Planck+DESI.

3.4. Effect of alternate assumptions: the distribution of DM_{HG} and σ_{IGM}

It is worth underscoring that the likelihood function for the BINGO FRB simulated data is highly dependent on some astrophysical distributions and properties of the respective FRBs. One important point to note is that the likelihood function incorporates the distribution of the mean DM_{HG}, stemming from galaxy evolution and formation. In a real analysis, we would attempt to model this distribution and choose, maybe with the aid of a statistical tool such as the evidence, the best model that fits the data. However, in this analysis, we simply simulate DM_{HG} as the simplest Gaussian distribution to test how cosmological parameters are affected by different likelihoods.

We consider two different Gaussian distributions, namely, $N(100, 50)$ and $N(100, 20)$. We compare in Fig. 8 the respective contours produced in previous sections, changing only the likelihood, which relates to the assumed distribution of the host galaxy DM. As we can see, the distribution does affect the contours as expected. Also, we find that the lognormal case, which has been used in the main body of the paper, is less well-constraining than assuming that the distribution from Gaussian ones. Presumably, because the log-normal distribution has a less compact distribution of values as opposed to the Gaussian distribution, it would have fewer outliers in terms of high DMs arising from the host galaxy. This more compact distribution presumably produces less degeneracy with the effect that the cosmological parameters have on the likelihood of degeneracy we have with these parameters. More specifically, these roughly halve the constraints we find on the $w - H_0$ plane, as we can see from the top panel of the figure. This means that if the real distributions of DM from host galaxies are more compact than an assumed log-normal distribution, then the constraints provided by a BINGO FRB survey could be significantly better than the constraints yielded in this analysis.

We also investigate the effect that the bias parameter. We can see from Fig. 9 what effect the bias parameters, which effectively modulates the value of the actual σ_{IGM}, has in the parameter constraint. Given that the bias parameter modifies how much the DM



Fig. 8. Compare Lognormal with Gaussian distribution of DM_{HG} in wCDM model. Also, marginalized posterior distributions of the (w_0, w_a) parameters are compared for various distribution of DM_{HG} in w_0w_a model, including Lognormal, Gaussian $N(100, 50)$ and Gaussian $N(100, 20)$.

follows the distribution of dark matter in the Universe, a change in bias is equivalent to having a different power spectrum with

changed amplitude for the distribution of free electrons in our Universe and therefore, a larger bias implies a larger scatter of the actual values of the DM measured in the FBR mock data. We can see the equivalent effect in the Fig. 10. A smaller value for the bias implies on tighter constraints, which we can see from the parameter degeneracy between Ω_b and H_0. It is worth noting that according to some analysis, the value of this bias should indeed be less than one for a real data analysis.
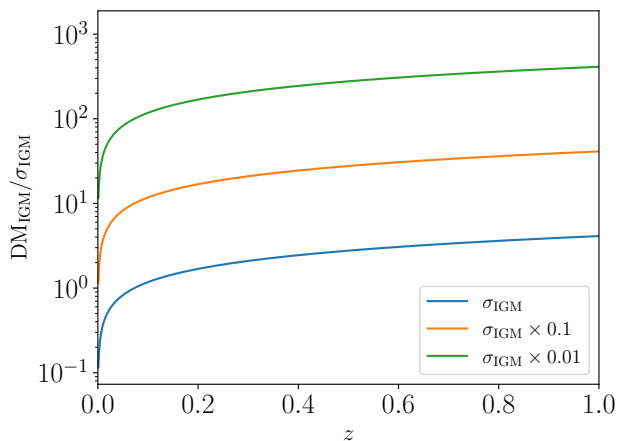
Fig. 9. The evolution of DM_{IGM}/σ_{IGM} with redshift z according to different bias factor b.
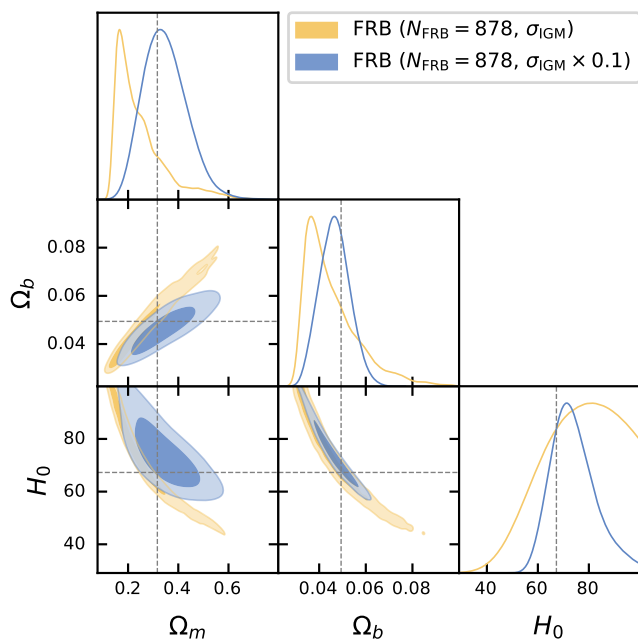
Fig. 10. Comparison of the result using σ_{IGM} and $0.1\sigma_{IGM}$, namely using a different bias factor b.

4. Conclusion

In this paper, we have taken simulated FRB mock datasets that we expect to have with a BINGO survey. We have assumed such FRBs are located in the sky via the Bingo Interferometric System (BIS) to a good enough accuracy that the host galaxy and, therefore, the host redshift can be identified in the catalog. This

in itself is a great effort that would have to be done by the collaboration in terms of both detection and follow-up of the survey.

We have shown that depending on the number of outriggers and technology of the outriggers used in different scenarios, an expected number of sources detected can range from a hundred to almost a thousand FBRs with a full survey, we further show that these sources can provide us with significant astrophysical and cosmological information.

A survey of even a hundred FRBs, such as the most conservative estimate for the BIS, can yield a self-consistent measurement of the astrophysical properties of the DM of galaxies and its scatter. This should be of great importance to galaxy formation as it would unveil the physics behind the content of electrons, the free electrons density within the host galaxies at cosmological redshift.

We also find that the FRBs from a BIS can complement the CMB data in the same way that SNIa and BAO do. Therefore, with good enough data, we can help shed light on interesting problems within the cosmological model today, such as the actual evolution of the dark energy equation of state, and we can also help shed light on the actual value of the Hubble constant.

We conclude that the data provided by a BIS can greatly help us further understand the mysteries of the Universe and help our understanding of galaxy formation as well as the nature of the components of our Universe.

References

Abdalla, E. & Marins, A. 2020, Int. J. Mod. Phys. D, 29, 2030014
Abdalla, E., Marins, A., Abdalla, F., et al. 2024, BINGO-ABDUS: A Radiotelescope to Unveil the Dark Sector of the Universe, ed. E. Papantonopoulos & N. Mavromatos (Cham: Springer Nature Switzerland), 311–326
Abdalla, E. et al. 2022a, Astron. Astrophys., 664, A14
Abdalla, F. B. et al. 2022b, Astron. Astrophys., 664, A16
Aghanim, N. et al. 2020a, Astron. Astrophys., 641, A5
Aghanim, N. et al. 2020b, Astron. Astrophys., 641, A6, [Erratum: Astron.Astrophys. 652, C4 (2021)]
Alam, S. et al. 2017, Mon. Not. Roy. Astron. Soc., 470, 2617
Amiri, M. et al. 2021, Astrophys. J. Supp., 257, 59
Amiri, M. et al. 2024, Astrophys. J., 969, 145
Bassa, C. G. et al. 2017, Astrophys. J. Lett., 843, L8
Beutler, F., Blake, C., Colless, M., et al. 2011, Mon. Not. Roy. Astron. Soc., 416, 3017
Bhandari, S. & Flynn, C. 2021, Universe, 7, 85
Bochenek, C. D., Ravi, V., Belov, K. V., et al. 2020, Nature, 587, 59
Caleb, M., Flynn, C., Bailes, M., et al. 2016, Mon. Not. Roy. Astron. Soc., 458, 708
Chatterjee, S. et al. 2017, Nature, 541, 58
Chawla, P. et al. 2022, Astrophys. J., 927, 35
Chevallier, M. & Polarski, D. 2001, Int. J. Mod. Phys. D, 10, 213
Connor, L., Sievers, J., & Pen, U.-L. 2016, Mon. Not. Roy. Astron. Soc., 458, L19
Cook, A. M. et al. 2023, Astrophys. J., 946, 58
Cordes, J. M. & Chatterjee, S. 2019, Ann. Rev. Astron. Astrophys., 57, 417
Cordes, J. M. & Lazio, T. J. W. 2002 [arXiv:astro-ph/0207156]

Cordes, J. M. & Lazio, T. J. W. 2003 [arXiv:astro-ph/0301598]
Cordes, J. M. & Wasserman, I. 2016, Mon. Not. Roy. Astron. Soc., 457, 232
Costa, A. A. et al. 2022, Astron. Astrophys., 664, A20
Deng, W. & Zhang, B. 2014, Astrophys. J. Lett., 783, L35
Dennison, B. 2014, Mon. Not. Roy. Astron. Soc., 443, 11
dos Santos, M. V. et al. 2024, Astron. Astrophys., 681, A120
Falcke, H. & Rezzolla, L. 2014, Astron. Astrophys., 562, A137
Gelman, A. & Rubin, D. B. 1992, Statist. Sci., 7, 457
Hashimoto, T. et al. 2022, Mon. Not. Roy. Astron. Soc., 511, 1961
James, C. W., Prochaska, J. X., Macquart, J. P., et al. 2021, Mon. Not. Roy. Astron. Soc., 509, 4775
Jaroszynski, M. 2019, Mon. Not. Roy. Astron. Soc., 484, 1637
Keane, E. F., Stappers, B. W., Kramer, M., & Lyne, A. G. 2012, Mon. Not. Roy. Astron. Soc., 425, 71
Keating, L. C. & Pen, U. L. 2020, Mon. Not. Roy. Astron. Soc., 496, L106–L110
Law, C. J. et al. 2017, Astrophys. J., 850, 76
Lemos, T., Gonçalves, R. S., Carvalho, J. C., & Alcaniz, J. S. 2023a, Eur. Phys. J. C, 83, 138
Lemos, T., Gonçalves, R. S., Carvalho, J. C., & Alcaniz, J. S. 2023b, Eur. Phys. J. C, 83, 1128
Lewis, A. & Bridle, S. 2002, Phys. Rev. D, 66, 103511
Lewis, A., Challinor, A., & Lasenby, A. 2000, Astrophys. J., 538, 473
Lin, H.-N. & Sang, Y. 2020, Mon. Not. Roy. Astron. Soc., 491, 2156
Lin, H.-N. & Sang, Y. 2021, Chin. Phys. C, 45, 125101
Lin, H.-N., Tang, L., & Zou, R. 2023, Mon. Not. Roy. Astron. Soc., 520, 1324
Lin, H.-N. & Zou, R. 2024, Astrophys. J., 962, 73
Linder, E. V. 2003, Phys. Rev. Lett., 90, 091301
Lorimer, D. R., Bailes, M., McLaughlin, M. A., Narkevic, D. J., & Crawford, F. 2007, Science, 318, 777
Luo, R., Lee, K., Lorimer, D. R., & Zhang, B. 2018, Mon. Not. Roy. Astron. Soc., 481, 2320
Luo, R., Men, Y., Lee, K., et al. 2020, Mon. Not. Roy. Astron. Soc., 494, 665
Macquart, J. P. et al. 2020, Nature, 581, 391
McQuinn, M. 2014, Astrophys. J. Lett., 780, L33
Niu, C. H. et al. 2022, Nature, 606, 873, [Erratum: Nature 611, E10 (2022)]
Petroff, E., Barr, E. D., Jameson, A., et al. 2016, Publ. Astron. Soc. Austral., 33, e045
Petroff, E., Hessels, J. W. T., & Lorimer, D. R. 2019, Astron. Astrophys. Rev., 27, 4
Petroff, E., Hessels, J. W. T., & Lorimer, D. R. 2022, Astron. Astrophys. Rev., 30, 2
Platts, E., Weltman, A., Walters, A., et al. 2019, Phys. Rept., 821, 1
Prochaska, J. X. & Zheng, Y. 2019, Mon. Not. Roy. Astron. Soc., 485, 648–665
Qiang, D.-C., Deng, H.-K., & Wei, H. 2020, Class. Quant. Grav., 37, 185022
Qiang, D.-C. & Wei, H. 2020, JCAP, 04, 023
Qiu, X.-W., Zhao, Z.-W., Wang, L.-F., Zhang, J.-F., & Zhang, X. 2022, JCAP, 02, 006
Ravi, V. 2019, Astrophys. J., 872, 88
Romero, G. E., del Valle, M. V., & Vieyro, F. L. 2016, Phys. Rev. D, 93, 023001
Ross, A. J., Samushia, L., Howlett, C., et al. 2015, Mon. Not. Roy. Astron. Soc., 449, 835
Sang, Y. & Lin, H.-N. 2022, Mon. Not. Roy. Astron. Soc., 510, 1801
Sang, Y. & Lin, H.-N. 2023, Mon. Not. Roy. Astron. Soc., 523, 5430
Sang, Y. & Lin, H.-N. 2024, Mon. Not. Roy. Astron. Soc., 533, 872
Scolnic, D. M. et al. 2018, Astrophys. J., 859, 101
Spitler, L. G. et al. 2016, Nature, 531, 202
Tang, L., Lin, H.-N., & Li, X. 2023, Chin. Phys. C, 47, 085105
Tendulkar, S. P. et al. 2017, Astrophys. J. Lett., 834, L7
Thornton, D. et al. 2013, Science, 341, 53
Totani, T. 2013, Pub. Astron. Soc. Jpn., 65, L12
Vieyro, F. L., Romero, G. E., Bosch-Ramon, V., Marcote, B., & del Valle, M. V. 2017, Astron. Astrophys., 602, A64
Walker, C. R. H., Ma, Y.-Z., & Breton, R. P. 2020, Astron. Astrophys., 638, A37
Walters, A., Ma, Y.-Z., Sievers, J., & Weltman, A. 2019, Phys. Rev. D, 100, 103519
Walters, A., Weltman, A., Gaensler, B. M., Ma, Y.-Z., & Witzemann, A. 2018, Astrophys. J., 856, 65
Wang, B., Abdalla, E., Atrio-Barandela, F., & Pavon, D. 2016a, Rept. Prog. Phys., 79, 096901
Wang, B., Abdalla, E., Atrio-Barandela, F., & Pavón, D. 2024, Rept. Prog. Phys., 87, 036901
Wang, B., Wei, J.-J., Wu, X.-F., & López-Corredoira, M. 2023a, JCAP, 09, 025
Wang, F. Y. & Yu, H. 2017, JCAP, 03, 023
Wang, J.-S., Yang, Y.-P., Wu, X.-F., Dai, Z.-G., & Wang, F.-Y. 2016b, Astrophys. J. Lett., 822, L7
Wang, Z.-H., Sang, Y., & Zhang, X. 2023b, Res. Astron. Astrophys., 23, 025002
Wu, Q., Yu, H., & Wang, F. Y. 2020, Astrophys. J., 895, 33
Wuensche, C. A. et al. 2022, Astron. Astrophys., 664, A15
Xu, H. et al. 2022, Nature, 609, 685
Xu, J. & Han, J. L. 2015, Res. Astron. Astrophys., 15, 1629
Xu, J. et al. 2023, Universe, 9, 330
Yang, Y.-P. & Zhang, B. 2016, Astrophys. J. Lett., 830, L31
Yao, J. M., Manchester, R. N., & Wang, N. 2017, Astrophys. J., 835, 29
Yu, H. & Wang, F. Y. 2017, Astron. Astrophys., 606, A3
Zhang, B. 2014, Astrophys. J. Lett., 780, L21
Zhang, B. 2023, Rev. Mod. Phys., 95, 035005
Zhang, G. Q., Yu, H., He, J. H., & Wang, F. Y. 2020, Astrophys. J., 900, 170
Zhang, J.-G., Zhao, Z.-W., Li, Y., et al. 2023, Sci. China Phys. Mech. Astron., 66, 120412
Zhao, Z.-W., Li, Z.-X., Qi, J.-Z., et al. 2020, Astrophys. J., 903, 83
Zhao, Z.-W., Wang, L.-F., Zhang, J.-G., Zhang, J.-F., & Zhang, X. 2023, JCAP, 04, 022
Zhu, C. & Zhang, J. 2022, Phys. Rev. D, 106, 023513

1 Center for Gravitation and Cosmology, College of Physical Science and Technology, Yangzhou University, Yangzhou 225009, China
2 Instituto de Física, Universidade de São Paulo, R. do Matão, 1371 - Butantã, 05508-09 - São Paulo, SP, Brazil
3 Department of Astronomy, School of Physical Sciences, University of Science and Technology of China, Hefei, Anhui 230026, China
4 CAS Key Laboratory for Research in Galaxies and Cosmology, University of Science and Technology of China, Hefei, Anhui 230026, China
5 School of Astronomy and Space Science, University of Science and Technology of China, Hefei, Anhui 230026, China
6 Department of Physics and Electronics, Rhodes University, PO Box 94, Grahamstown, 6140, South Africa
7 Universidade Estadual da Paraiba, Rua Baraúnas, 351, Bairro Universitário, Campina Grande-PB
8 Departamento de Física, Centro de Ciências Exatas e da Natureza - CCEN, Universidade Federal da Paraíba - UFPB ‖ CEP 58059-970 – João Pessoa - PB
9 Unidade Acadêmica de Física, Universidade Federal de Campina Grande, R. Aprígio Veloso, Bodocongó, 58429-900 - Campina Grande, PB, Brazil
10 College of Physics, Nanjing University of Aeronautics and Astronautics, Nanjing 211106, China
11 Instituto Federal de Educação, Ciência e Tecnologia de Minas Gerais, Campus Itabirito, Itabirito 35450-000, Brazil
12 Departamento de Física, Universidade Federal da Paraíba, Caixa Postal 5008, João Pessoa 58051-900, Paraíba, Brazil
13 Technische Universität München, Physik-Department T70, James-Franck-Strasse 1, 85748, Garching, Germany
14 Institute of Cosmology and Gravitation, University of Portsmouth, Dennis Sciama Building, Portsmouth PO1 3FX, United Kingdom
15 School of Aeronautics and Astronautics, Shanghai Jiao Tong University, Shanghai 200240, China
16 Instituto Nacional de Pesquisas Espaciais - INPE, Av. dos Astronautas 1758, Jardim da Granja, São José dos Campos, SP, Brazil
17 Centro de Gestão e Estudos Estratégicos - CGEE, SCS, Qd 9, Lote C, Torre C S/N, Salas 401 - 405, 70308-200 - Brasília, DF, Brazil
18 Instituto de Física, Universidade de Brasília, Campus Universitário Darcy Ribeiro, 70910-900 - Brasília, DF, Brazil
19 Shanghai Astronomical Observatory, Chinese Academy of Sciences, Shanghai 200030, China
20 Unidade Acadêmica de Engenharia Elétrica, Universidade Federal de Campina Grande, R. Aprígio Veloso, Bodocongó, 58429-900 Campina Grande, PB, Brazil
21 Department of Physics and Astronomy, Sejong University, Seoul, 143-747, Korea